Proceedings of the ASME 2016 International Dynamic Systems and Control Conference
DSCC 2016
October 12-14, 2016, Minneapolis, USA

DSCC2016-9705

PID SLIDING MODE CONTROL OF PROLATE FLEXIBLE PNEUMATIC ACTUATORS

Jonathon E. Slightam
Department of Mechanical Engineering
Marquette University
Milwaukee, WI 53233
Email: jonathon.slightam@mu.edu

Mark L. Nagurka
Department of Mechanical Engineering
Marquette University
Milwaukee, WI, 53233
mark.nagurka@mu.edu

ABSTRACT

The inherent compliance, high power-density, and muscle-like properties of soft actuators are especially attractive and useful in many applications, including robotics. In comparison to classical/modern control approaches, model-based control techniques, e.g., sliding mode control (SMC), applied to flexible fluidic actuators (FFAs) offer significant performance advantages and are considered to be state-of-the-art. Improvements in position tracking are possible using nonlinear control approaches that offer enhanced performance for common applications such as tracking of sinusoidal trajectories at high frequencies.

This paper introduces a SMC approach that increases the tracking capabilities of prolate flexible pneumatic actuators (PFPAs). A model-based proportional, integral, derivative sliding mode control (PIDSMC) approach designed for position control of PFPAs is proposed. SMC and PIDSMC systems are implemented on low-cost open-source controls hardware and tested for tracking sinusoidal trajectories at frequencies of 0.5 Hz and 1.0 Hz with an amplitude of 8.255 mm and an offset of 12.7 mm. The PIDSMC approach reduced the maximum tracking error by 20.0%, mean error by 18.6%, and root-mean-square error by 10.5% for a 1 Hz sinusoidal trajectory and by 8.7%, 14.7%, and 3.8%, respectively, for a 0.5 Hz sinusoidal trajectory. These reductions in tracking errors demonstrate performance advantages of the PIDSMC over conventional sliding mode position controllers.

INTRODUCTION

A prolate flexible pneumatic actuator (PFPA) is a tube of hyperelastic material within a sleeve of braided polymer. When pressurized with compressed air, the composite tube inflates circumferentially and contracts longitudinally resulting in a force and displacement that is analogous to muscle [1]. These types of actuators are sometimes called pneumatic artificial muscles (or McKibben actuators), where a flexible fluidic actuator (FFA) describes the actuation type and prolate identifies the geometric aspect ratio of the device [2]. This paper presents the motivation and background to inspire a new class of controlled actuators for robotics and many other applications.

PFPAs offer unrivaled power density, with values reported from 5 - 10 kW/kg [1], [3]. Moreover, they can achieve high forces at relatively low pressures that are typically available in labs, schools, and hospitals. PFPAs are controllable nonlinear springs, i.e., their output force is both pressure and position dependent. This property makes them ideal for biologically-inspired applications, mobile robots, and human assistive devices (prosthetics and orthotics) [4]. This paper sets the stage for improvements in motion control for these applications.

BACKGROUND

PFPAs were modeled by describing the change in enthalpy in the control volume [5], [2]. Using this approach Henry Paynter demonstrated accurate open-loop control with experimentally determined parameters [6]. Applications of this work include vehicle suspensions and engine mount vibration dampening [7]. Caldwell illustrated that closed-loop control could be achieved using discrete linear feedback control theory [8].

Model-based nonlinear control techniques have proven to be practical and superior in many cases to linear

control theory for pneumatic and highly nonlinear motion control applications. Sliding mode control (SMC) has been a topic of substantial research, especially in applied fluid power applications such as the motion control of FFAs. SMC approaches have seen many successes due to their ability to mathematically converge the error dynamics to zero over a given trajectory and implement high speed digital switching that enables powerful and robust tracking behavior [9]. For example, Comber *et al.* successfully applied a sliding mode position controller on a pneumatic five degree-of-freedom (DOF) magnetic resonance imaging (MRI) compatible steerable needle robot that exhibited needle tip errors of 0.78 mm or less, smaller than the voxel size of most MRI machines [10]. De Volder *et al.* illustrated positioning accuracy of ± 30 μm using a PI sliding mode controller [11]. Additionally, SMC systems have been implemented on hydraulic manipulators and chemically powered pneumatic FFAs [12], [13].

Some literature points out the limited performance using linear control theory for FFAs. Surdilovic *et al.* used linear control theory for motion control of flexible pneumatic actuators reporting a low position accuracy of 10 mm [14]. Linear control theory applied to the motion control of FFAs exhibited significant overshoot (12%) and was sensitive to noise, changes in supply pressure, temperature, and pipe length [8]. Undesirable steady-state errors were achieved using PI position control in antagonistic pairs of PFPAs, while also suggesting implementing nonlinear control methods [15]. In contrast, SMC approaches show substantial tracking improvements when compared to classical PID controllers for PFPAs [16].

Model-based control of soft actuators such as FFAs is of high interest in current research and was identified as one of the top scientific needs to realize human-robot interaction by *2015 Multi-Annual Roadmap for Robotics in Europe* [17]. Lilly *et al.* developed and simulated a sliding mode angular position controller for an antagonistic pair of PFPAs and reported an approximate maximum tracking error of 1.15 deg with a 20 kg payload [18]. Comber *et al.* reported a maximum steady-state error of 0.015 mm using sliding mode position control of an oblate flexible pneumatic needle driver [19]. Nakamura *et al.* used model-based force and position control of PFPAs reinforced with glass fibers [20].

Applications in multi-DOF systems further show the capabilities of model-based control techniques for prolate and oblate FFAs. A haptic device made using a delta robot driven by PFPAs implemented position and stiffness control with a PI computed torque and stiffness control method, resulting in an average maximum position error of 1.17 mm [21]. Sardellitti reported sliding mode torque and stiffness control for antagonistically actuated contractile flexible pneumatic pairs that experimentally confirmed excellent tracking, i.e., maximum error of 0.12 N-m and 0.06 N-m/rad for torque and stiffness tracking, respectively [22]. Ugurlu *et al.* described a novel torque and force control using feedback linearization to be implemented in future exoskeleton systems [23]. Driver and Shen tested a SMC system on a hybrid sleeve flexible pneumatic actuator that exhibited approximately a maximum of 3 deg tracking error when following a sinusoid wave at 1 Hz and an angular amplitude of 20 deg [24]. A maximum of 0.41 deg tracking error resulted when using a sliding mode position controller on an oblate rotary flexible pneumatic actuator [25]. Ivlev reported that along with the precise control of oblate rotary flexible pneumatic actuators in [25], the inherent compliance would be suitable for safe human-robot interaction, e.g., exoskeletons [26].

This paper is motivated by significant errors presented in the tracking of sinusoidal trajectories about their inflection points, especially at higher frequencies (1 Hz or greater) as illustrated by experimental results in [18], [24], and [16]. This paper presents a similar modeling approach taken by Comber *et al.* and Driver *et al.* and uses experimental methods to accurately model the highly nonlinear behavior of PFPAs [19], [24]. Furthermore, a sliding mode position controller is derived from the actuator and pressure dynamics while introducing proportional, integral, and derivative gain action to the SMC as done with the PI SMC in [11] and alternatively to the Fuzzy SMC presented in [27] to eliminate the errors about inflection points in sinusoidal tracking problems.

MODELING

Actuator Dynamics

A diagram of the PFPA system being modeled and controlled is illustrated in Figure 1. The model of the system is shown in Figure 2 The length L of the PFPA is defined by

$$L = L_0 - x. \tag{1}$$

where L_0 is the initial length and x is the translation of the free end of the FFA. L is also related to the fiber helical fiber length, b, and angle of the fiber relative primary axis by $L = bcos(\theta)$. The force from the FFA, F, as a result of pressurization is the sum of the force acting on the end caps, F_1, and the reaction force of the hyperelastic tube being deformed, F_2,

$$F = \Sigma F = F_1 + F_2. \tag{2}$$

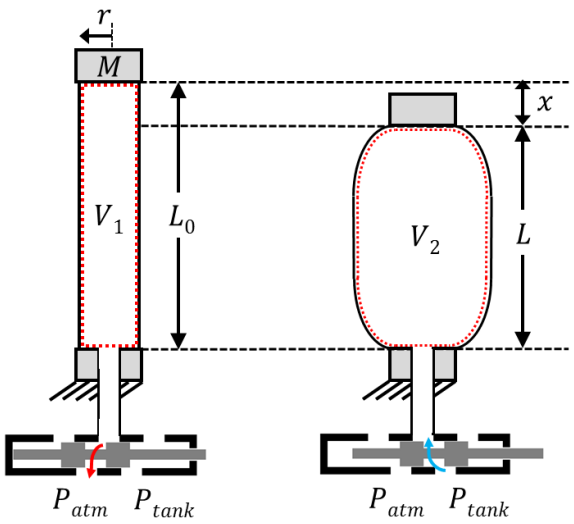

FIGURE 1. PFPA SYSTEM DIAGRAM.

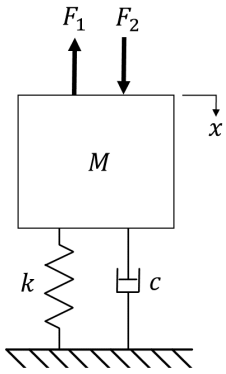

FIGURE 2. PFPA FREE-BODY-DIAGRAM.

The forces acting on the FFA, derived using the principle of virtual work, are

$$F_1 = -\frac{dV_1}{dL}P, \quad F_2 = -\frac{dV_2}{dL}P, \tag{3}$$

where V_1 is the control volume for the force acting on the caps and V_2 is the control volume for the force from the deformation of the bladder. Since the volume of control volume 2 as a function of actuator length, L, is $L(b^2 - L^2)/(4\pi n^2)$, the force from the pressure then becomes

$$F = \frac{P(3L^2 - b^2)}{4\pi n^2}. \tag{4}$$

This force represents the input to the equation of motion that is written by applying Newton's second law to the system, resulting in

$$M\ddot{x} + c\dot{x} + kx = F, \tag{5}$$

where k is the stiffness of the actuator material, c is the viscous damping coefficient, and M is the mass of the non-fixed end of the PFPA. From mechanics of materials, the stiffness of axial deflection of a tube from an internal pressure can be expressed as

$$k_L = \frac{tE}{rL_0}\left(2 - \frac{1}{\nu}\right), \tag{6}$$

where E is the actuator's Young's modulus, r is the actuator mean radius, ν is Poisson's ratio of the material, and t is the thickness of the tube [28]. This approach has been used for oblate FFAs [19], [29].

Linear theory can not sufficiently describe the axial displacement of the PFPA due to the nonlinear material and nonlinear deformation effects. An efficient way to address this is by using experimental methods. Writing Equation 6 as a 4th-order polynomial, the stiffness can be approximated with the linear theory in Equation 6 to match that of the nonlinear material and nonlinear deformation phenomenon by

$$k = \frac{tE}{rL_0}\left(2 - \frac{1}{\nu}\right)\left(\lambda_4 x^4 + \lambda_3 x^3 + \lambda_2 x^2 + \lambda_1 x + \lambda_0\right). \tag{7}$$

Substituting Equations 4 and 7 into Equation 5 gives the equation of motion,

$$M\ddot{x} + c\dot{x} + kx = \frac{P(3L^2 - b^2)}{4\pi n^2}, \tag{8}$$

where the nonlinear stiffness coefficient is given by Equation 7. The actuator model parameters are listed in Table 1.

Pressure and Mass Flow Dynamics

The pneumatic system is modeled for the actuator control volume with a proportional flow control valve. The pressure dynamics of the PFPA control volume is the time derivative of the ideal gas law, giving:

$$\dot{P} = \frac{RT}{V}\dot{m} - \frac{P}{V}\dot{V}, \tag{9}$$

TABLE 1. ACTUATOR PARAMETERS.

Parameter	Value	Parameter	Value
M	0.05 kg	λ_0	18.2
c	0.44 N-s/mm	λ_1	-4.72 mm^{-1}
L_0	127 mm	λ_2	0.430 mm^{-2}
b	151.9 mm	λ_3	-0.0184 mm^{-3}
n	1	λ_4	0.000339 mm^{-4}
r	7.62 mm	E	3447 kPa
t	3.175 mm	ν	0.49

where R is the universal gas constant for air, T is the temperature of the air, V is the volume of the actuator, $\dot{V}$ is the rate of change of volume, and $\dot{m}$ is the mass flow dynamics. The pressure dynamics are assumed to be isothermal and the mathematical models are explained in more detail in [10], [19], [30] and [31]. The mass flow dynamics are modeled as isentropic flow through a plate with a small hole (aperture), the mass flow is a function of the aperture cross-sectional area of the spool valve, and the area normalized flow, Ψ, as described by

$$\dot{m} = A_v \Psi, \tag{10}$$

where the valve dynamics are assumed to be idealized and the aperture area A_v is assumed to be linearly proportional to the control command signal, u. The area normalized mass flow is a piecewise function governed by choked and unchoked flow regimes that is based on the quotient of the downstream and upstream pressures, respectively.

$$\Psi(P_u, P_d) = \begin{cases} \Psi_c & \frac{P_d}{P_u} \leq C_r \quad Choked \\ \Psi_{uc} & \frac{P_d}{P_u} > C_r \quad Unchoked \end{cases} \tag{11}$$

where Ψ_c is the choked area normalized mass flow defined by,

$$\Psi_c = \frac{C_1 C_f P_u}{\sqrt{T}}, \tag{12}$$

and Ψ_{uc} is the unchoked area normalized mass flow defined by,

$$\Psi_{uc} = \frac{C_2 C_f P_u}{\sqrt{T}} \left(\frac{P_d}{P_u}\right)^{1/\gamma} \sqrt{1 - \left(\frac{P_d}{P_u}\right)^{(\gamma-1)/\gamma}}. \tag{13}$$

The coefficients C_1 and C_2 are gas properties, C_f is a nondimensional discharge coefficient, and C_r is the threshold between choked and unchoked flow through the valve. For air, C_r is 0.528, C_f is 0.2939, where C_1 and C_2 are defined by

$$C_1 = \sqrt{\frac{\gamma}{R} \frac{2}{\gamma+1}^{\frac{\gamma+1}{\gamma-1}}}, \tag{14}$$

and

$$C_2 = \sqrt{\frac{2\gamma}{R(\gamma-1)}}. \tag{15}$$

For the internal chamber and the type of valve used (5-3 proportional flow control valve), Ψ is governed by

$$\Psi(P_1, P_{source}, P_{atm}) = \begin{cases} P_d = P_1, P_u = P_{source} & A_v \geq 0 \\ P_d = P_{atm}, P_u = P_1 & A_v < 0. \end{cases} \tag{16}$$

The volume inside the actuator as a function of length is

$$V = \frac{L(b^2 - L^2)}{4\pi n^2}, \tag{17}$$

and the time rate of change in volume is

$$\dot{V} = \frac{b^2 - 3L^2}{4\pi n^2} \dot{L}. \tag{18}$$

The pressure dynamics substituted in the equation of motion gives the third-order nonlinear dynamics,

$$M\dddot{x} + c\ddot{x} + k\dot{x} = \dot{F}. \tag{19}$$

The pneumatic system parameters are summarized in Table 2.

CONTROLLER DESIGN

The SMC is made of two components that make a 3rd-order control law, one term is the equivalent control and the other is the robustness control to deal with model uncertainties and system disturbances [9].

$$u = u_{eq} + u_{rb} \tag{20}$$

TABLE 2. PNEUMATIC SYSTEM PARAMETERS.

Parameter	Value	Parameter	Value
P_{tank}	441.3 kPa	A_v	$\pm$ 5.161 mm^2
P_{atm}	101.3 kPa	C_d	0.5898
R	287.1 J kg^{-1} K^{-1}	C_f	0.2800
C_1	0.04040	T	273.0 K
C_2	1.156	γ	1.400

where the equivalent control is obtained from the system model that includes the pressure dynamics and is given in Equation 19 and where $\dot{F}$ is the time derivative of Equation 4, resulting in

$$\dot{F} = \frac{6LP\dot{L}}{2\pi n^2} + \frac{3L^2 - b^2}{4\pi n^2}\dot{P}. \tag{21}$$

Including the pressure dynamics from Equation 12 and substituting the volume and volume dynamics from Equations 17 and 18, respectively, with simplification gives

$$\dot{F} = \frac{3LP}{2\pi n^2}\dot{L} + \frac{P(3L^2 - b^2)^2}{4\pi n^2(b^2L - L^3)}\dot{L} + \frac{3L^2 - b^2}{b^2L - L^3}RT\dot{m}. \tag{22}$$

Rearranging Equation 19 with the expansion of Equation 22 included on the right-hand side to solve for $\dddot{x}$ results in

$$\dddot{x} = \frac{1}{M}\left(\frac{3LP\dot{L}}{2\pi n^2} + \frac{P(3L^2 - b^2)^2}{4\pi n^2(b^2L - L^3)}\dot{L} + \frac{3L^2 - b^2}{b^2L - L^3}RT\dot{m} - c\ddot{x} - k\dot{x}\right). \tag{23}$$

Further simplification is possible by separating terms that are not and are effected by the valve aperture area, A_v, respectively, resulting in

$$\hat{f} = \frac{1}{M}\left(\frac{3LP\dot{L}}{2\pi n^2} + \frac{P(3L^2 - b^2)^2}{4\pi n^2(b^2L - L^3)}\dot{L} - c\ddot{x} - k\dot{x}\right), \tag{24}$$

and

$$\hat{g} = \frac{1}{M}\left(\frac{3L^2 - b^2}{b^2L - L^3}RT\Psi\right). \tag{25}$$

For position control, a third-order sliding surface is described by

$$s = \left(\frac{d}{dt} + \lambda\right)^3 \int e = \ddot{e} + 3\lambda\dot{e} + 3\lambda^2 e + \lambda^3 \int e dt, \tag{26}$$

where $e = x - x_d$ and λ is a gain. A Lyapunov candidate function was chosen to be

$$V = \frac{1}{2}s^2. \tag{27}$$

Taking the time derivative of Equation 27, results in

$$\dot{V} = s\dot{s}, \tag{28}$$

which is set to be negative definite and $\dot{s} = sat(s/\phi)$, where ϕ is the robustness constant and $\dot{s}$ is bounded by ± 1. To force the error dynamics to smoothly converge to zero, the desired Lyapunov function is multiplied by a constant η. Factoring in the desired Lyapunov function and sliding surface with Equation 23 and substituting in Equations 24 and 25 and solving for the command signal, gives the closed-loop SMC law as

$$u = K_p \frac{\dddot{x}_D + \hat{f} - 3\lambda\ddot{e} - 3\lambda^2\dot{e} - \lambda^3 e - \eta sat(s/\phi)}{\hat{g}} \tag{29}$$

where K_p is a proportional gain and $\dddot{x}_D$ is the third derivative of the continuous desired trajectory. Adding integral and derivative action to the SMC law can improve tracking and response characteristics.

$$u_{PIDSMC} = K_i \int u dt + K_d \dot{u} \tag{30}$$

The controller parameters were experimentally determined by considering different trajectories for the SMC, resulting in the values listed in Table 3.

TABLE 3. SMC PARAMETERS.

Parameter	Value	Parameter	Value
K_p	1.00E-9	λ_x	125 Hz
ϕ	0.254 mm/s^2	η	1270 mm/s^3

The parameters of the PIDSMC system are listed in Table 4 and were experimentally determined using the same approach.

TABLE 4. PIDSMC PARAMETERS.

Parameter	Value	Parameter	Value
K_p	1.00E-9	λ_x	125 Hz
K_i	0.01	η	1270 mm/s^3
K_d	0.01	ϕ	0.254 mm/s^2

EXPERIMENTAL SETUP

For the experimental setup, a PFPA was configured in a test stand as shown in Figure 3 and its position measured with a spring returned string potentiometer. An Enfield Technologies LS-V05s proportional pneumatic control valve was used with a NPX MPX5700GP pressure sensor. An Arduino MEGA 2560 revision 3 microcontroller was used for control and data acquisition using Mathworks SIMULINK through a serial connection of a laptop computer running a MATLAB graphical user interface to acquire signals. The control program operated at 1000 Hz and the data sampling rate was approximately 50 Hz. The data sampling is significantly slower due to the serial interface and communication running within a MATLAB graphical user interface that is not operating at real-time speeds.

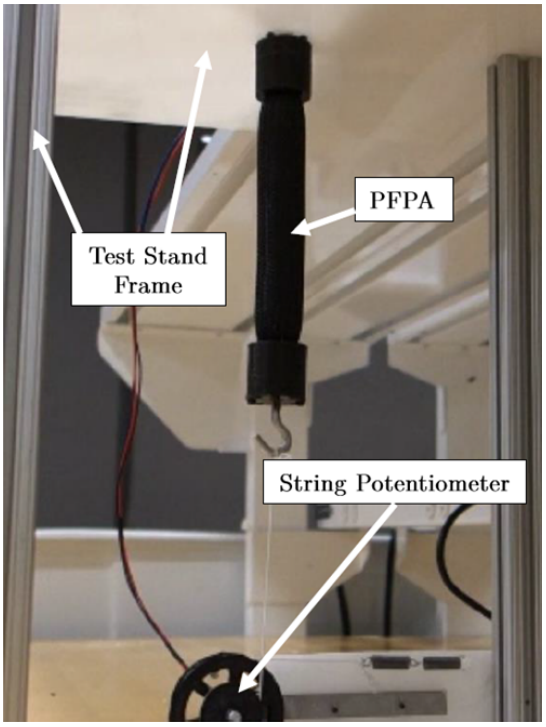

FIGURE 3. EXPERIMENTAL SETUP.

EXPERIMENTAL RESULTS

Model Validation

The nonlinear spring rate parameters listed in Table 1 were experimentally determined by pressurizing the actuator at a quasi-static rate. The model predictions were compared to the experimental results of the PFPA stiffness, as illustrated in Figure 4. The dynamic behavior of the actuator was also experimentally tested using a square wave input command to the proportional flow control valve. This same signal was then used as an input to the dynamic model developed for the PFPA, as shown in Figure 5.

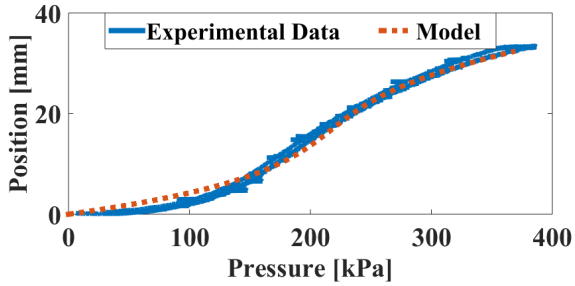

FIGURE 4. PFPA STIFFNESS.

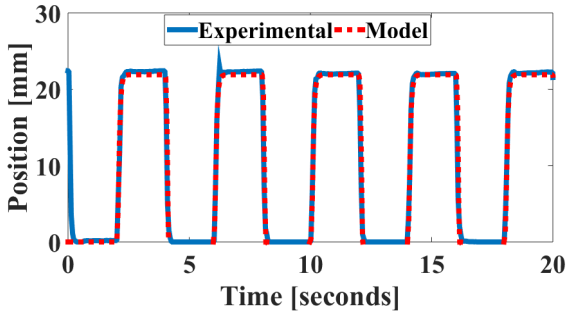

FIGURE 5. DYNAMIC SIMULATION VS. EXPERIMENT.

Control Experiments

Sinusoidal tracking experiments were conducted on SMC and PIDSMC systems after they were tuned. Tuning parameters were experimentally determined, as done

in [19], [10], and [29]. Tracking experiments at 0.5 Hz and 1.0 Hz were executed with a sinusoidal amplitude of 8.255 mm and an offset of 12.7 mm. A low-pass filter with a cut-off frequency of 20 Hz was implemented to filter out chattering from the SMC command signal and was experimentally determined. Moreover, the PIDSMC's derivative and integral gains were implemented after this filter, with the proportional gain being applied prior to the filter. Sinusoidal tracking of the SMC at 0.5 Hz is illustrated in Figure 6.

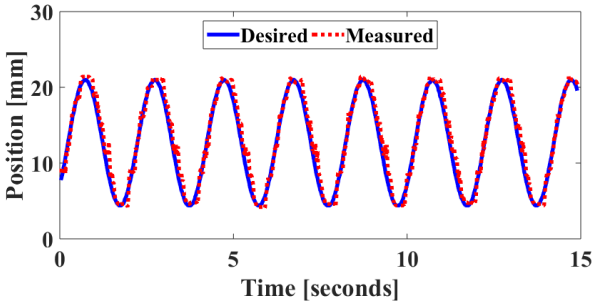

FIGURE 6. SMC TRACKING (0.5HZ).

The trajectory error over the time of the experiment is shown in Figure 7.

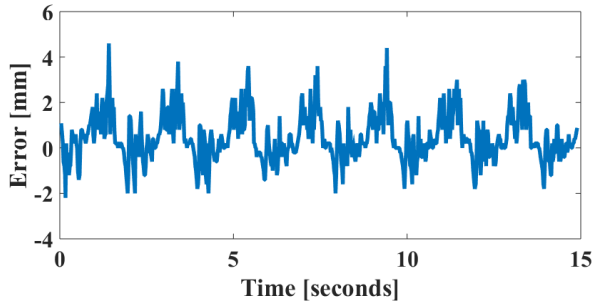

FIGURE 7. SMC TRACKING ERROR (0.5HZ).

The results of the SMC tracking a sinusoidal wave at 1.0 Hz are presented in Figure 8. Trajectory errors for sinusoidal tracking are illustrated in Figure 9. Figures 6 and 8 show the successful sinusoidal tracking from the SMC. The sinusoidal tracking experiment results of the PIDSMC at 0.5 Hz are depicted in Figure 10. The tracking errors over the time of the PIDSMC experiment are plotted in Figure 11. The results of the PIDSMC tracking a sinusoidal wave at 1.0 Hz are reported in Figure 12. Trajectory errors for

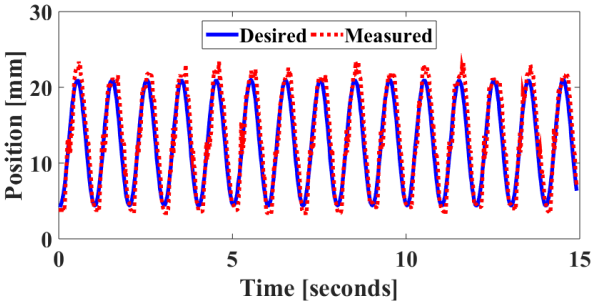

FIGURE 8. SMC TRACKING (1.0 HZ).

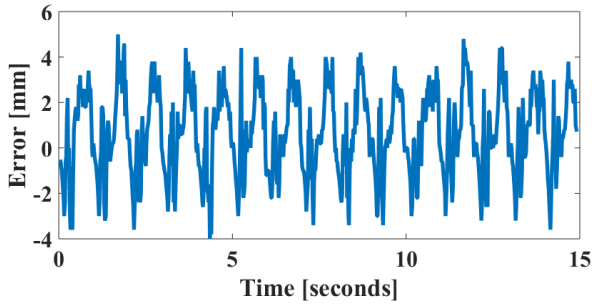

FIGURE 9. SMC TRACKING ERROR (1.0 HZ).

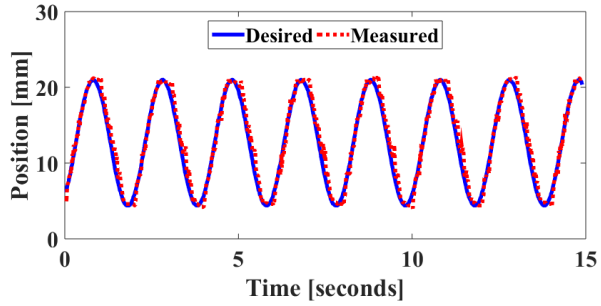

FIGURE 10. PIDSMC TRACKING (0.5HZ).

sinusoidal tracking are represented in Figure 13.

Mean tracking error, RMS tracking error, and the maximum tracking error are reported for both experiments when the measured signal is considered to be past the finite time reaching phase. These errors are summarized for both experiments in Table 5.

CONCLUSIONS

This paper reports the modeling and controller design for a single DOF PFPA. The PFPA is modeled using a lumped-parameter approach that utilizes a 4th-order polynomial modification of the linear axial deformation of a tube. This lumped-parameter and experimental approach

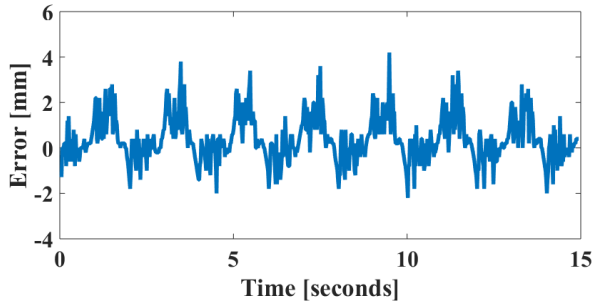

FIGURE 11. PIDSMC TRACKING ERROR (0.5HZ).

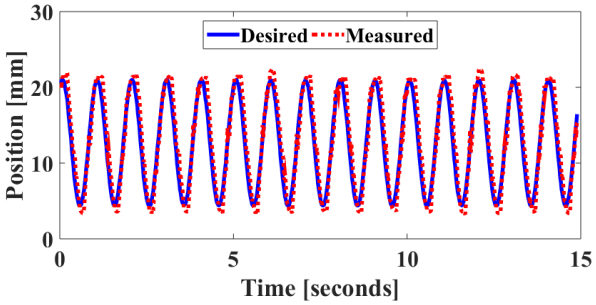

FIGURE 12. PIDSMC TRACKING (1.0 HZ).

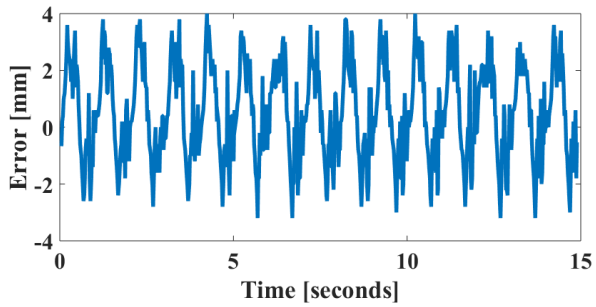

FIGURE 13. PIDSMC TRACKING ERROR (1.0 HZ).

TABLE 5. CONTROLLER PERFORMANCE SUMMARY.

Controller	RMS e	$\bar{e}$	Max e
SMC 0.5Hz	0.0105 mm	2.46E-5 mm	4.60 mm
SMC 1.0Hz	0.0153 mm	3.24E-5 mm	5.00 mm
PIDSMC 0.5Hz	0.0101 mm	2.10E-5 mm	4.20 mm
PIDSMC 1.0Hz	0.0137 mm	2.64E-5 mm	4.00 mm

accurately predicts the static and dynamic characteristics from a qualitative perspective, respectively. The introduction of the proportional, integral, and derivative gain action on top of the SMC has shown that sinusoidal tracking improvements are possible.

Control experiments demonstrate that a 3.81%, 8.70%, and 14.7% improvements in RMS, maximum, and mean errors, respectively, can be achieved using PIDSMC over SMC when tracking a sinusoid at 0.5 Hz. Improvements by 10.5%, 20.0%, and 18.6% were illustrated in RMS, maximum, and mean errors, respectively, using the PIDSMC over SMC for 1.0 Hz sinusoidal tracking.

Some chattering noise persisted despite using low-pass filters and trying many different tuning configurations. This is thought to be attributed to the performance limitations of the open-source microcontroller hardware used and some vibrations due to the experimental setup.

REFERENCES

[1] Hannaford, B., and Winters, J., 1990. *Actuator Properties and Movement Control: Biological and Technical Models*. Springer-Verlag, New York, ch. Multiple Muscle Systems: Biomechanics and Movement Organization, pp. 101–120.

[2] Paynter, H. M., 1996. "Thermodynamic Treatment of Tug-n-Twist Technology: Part 1. Thermodynamic Tugger Design". *Japan/USA Symposium on Flexible Automation*, ***1***, pp. 111–117.

[3] Caldwell, D. G., Razak, A., and Goodwin, M. J., 1993. "Braided Pneumatic Artificial Muscle Actuators". *IFAC Conference on Intelligent Autonomous Vehicles*, pp. 507–512.

[4] Gaiser, I., Wiegand, R., Ivlev, O., Andres, A., Breitweiser, H., Shulz, S., and Bretthauer, G., 2012. *Smart Actuation and Sensing Systems - Recent Advances and Future Challenges*. InTech, ch. Chapter 22: Compliant Robotics and Automation with Flexible Fluidic Actuators and Inflatable Structures, pp. 567–608.

[5] Paynter, H. M., and Jaurez, J., 2000. "Thermodynamic Analysis of Mechatronic Pnuematic Driven Spherical Joint". *IEEE/ASME Transactions on Mechatronics*, **5**(2).

[6] Paynter, H. M., and Jaurez, J., 1999. "Thermodynamic Treatment of Tug-n-Twist Technology Part 2: Thermodynamic Twistor Design". *IEEE/ASME International Conference on Advanced Intelligent Mechatronics*.

[7] Paynter, H. M., and Nagurka, M., 1997. "Hybrid Tension-Compression Pneumatic Actuators for Active Leveling, Tuning, and Damping of Vehicle Suspensions and Engine Mounts". *Proceedings of the 1997 IEEE Conference on Control Applications*, p. 630.

[8] Caldwell, D. G., Medrano-Cerda, G. A., and Goodwin, M. J., 1993. "Braided Pneumatic Actuator Control of a Multi-Jointed Manipulator". *Proceedings of the 1993 IEEE Conference on Systems, Man, and Cybernetics*, Oct. 17-20, pp. 423–428.

[9] Slotine, J., and Li, W., 1991. *Applied Nonlinear Control*. Prentice Hall.

[10] Comber, D. B., Barth, E. J., and Webster III, R. J., 2014. "Design and Control of an MR-Compatible Precision Pneuamtic Active Cannula Robot". *ASME Journal of Medical Devices,* ***8***(1).

[11] Volder, M. D., Coosemans, J., Puers, R., and Reynaerts, D., 2008. "Characterization and Control of a pneumatic microactuator with Integrated Inductive Position Sensor". *Journal of Sensors and Actuators,* ***141***(1), pp. 192–200.

[12] Indrawanto, I., 2011. "Sliding Mode Control of a Single Rigid Hydraulically Actuated Manipulator". *International Journal of Mechanical and Mechatronic Engineering,* ***11***(5).

[13] Shen, X., and Christ, D., 2011. "Design and Control of Chemomuscle: A Liquid-Propellent-Powered Muscle Actuation System". *ASME Journal of Dynamic Systems, Measurement, and Control,* ***133***(2).

[14] Surdivolic, D., Radojicic, J., Schulze, M., and Dembek, M., 2008. "Modular Hybrid Robots with Biologically Inspired Actuators and Joint Stiffness Control". *Proceedings of the 2nd Biennial IEEE/RAS-EMBS International Conference on Biomedical Robotics and Biomechatronics*, Oct. 19-22, pp. 289–294.

[15] Situm, Z., and Herceg, S., 2008. "Design and Control of a Manipulator Arm Driven by Pneumatic Muscle Actuators". *16th Mediterranean Conference on Control and Automation*, June 25-27, pp. 926–931.

[16] Liu, H., Zhao, Y., Jiang, F., and Yao, X., 2015. "Pneumatic Muscle Actuator Position Control Based on Sliding Mode Control Algorithms". *Proceedings of the 2015 IEEE International Conference on Information and Automation*, Aug. 8-10, pp. 1115–1120.

[17] The Partnership for Robotics In Europe, 2015. "Robotics 2020 Multi-Annual Roadmap for Robotics in Europe". *Technical Report*.

[18] Lilly, J., and Yang, L., 2005. "Sliding Mode Tracking for Pneumatic Muscle Actuators in Opposing Pair Configuration". *IEEE Transactions on Control Systems Technology,* ***13***(4), pp. 550–558.

[19] Comber, D. B., Slightam, J. E., Gervasi, V. R., Webster III, R. J., and Barth, E. J., 2013. "Design and Precision Control of an MR-Compatible Flexible Fluidic Actuator". *Proc. ASME/Bath Symposium on Fluid Power and Motion Control*, Oct. 6-9, pp. 1–9.

[20] Nakamura, T., and Shinohara, H., 2007. "Position and Force Control Based on Mathematical Models of Pneumatic Artificial Muscles Reinforced by Straight Glass Fibers". *2007 IEEE International Conference on Robotics and Automation*, April 10-14, pp. 4361–4366.

[21] Hirano, J., Tanaka, D., Watanabe, T., and Nakamura, T., 2014. "Development of Delta Robot Driven by Pneumatic Artificial Muscles". *2014 IEEE/ASME International Conference on Advanced Intelligent Mechatronics*, July 8-11, pp. 1400–1405.

[22] Sardenillitti, I., Palli, G., Tsagarakis, N. G., , and Caldwell, D. G., 2010. "Antagonistically Actuated Compliant Joint: Torque and Stiffness Control". *The 2010 IEEE/RSJ International Conference on Intelligent Robots and Systems*, Oct. 18-22, pp. 1909–1914.

[23] Ugurlu, B., Forni, P., Doppmann, C., and Morimoto, J., 2015. "Torque and Variable Stiffness Control for Antagonistically Driven Pneumatic Muscle Actuators via a Stable Force Feedback Controller". *2015 IEEE/RSJ International Conference on Intelligent Robots and Systems*, Sept. 28 - Oct. 2, pp. 1633–1639.

[24] Driver, T. A., and Shen, X., 2014. "Design and Control of a Sleeve Muscle-Actuated Robot Elbow". *ASME Journal of Dynamic Systems, Measurement, and Control,* ***136***(1).

[25] Mihajlov, M., H*ü*bner, M., Ivlev, O., and Gr*ä*ser, A., 2006. "Modeling and Control of Fluidic Robotic Joint with Natural Compliance". *Proceedings of the 2006 IEEE International Conference on Control Applications*, Oct. 4-6, pp. 2498–2503.

[26] Ivlev, O., 2009. "Soft Fluidic Actuators of Rotary Type for Safe Physical Human-Machine Interaction". *2009 IEEE 11th International Conference on Rehabilitation Robotics*, June 23-26.

[27] Qian, J., and Ri, S., 2015. "Adaptive Fuzzy Sliding Mode Control for Pneumatic Muscle Actuator". *Chinese Automation Congress (CAC)*, Nov. 27-29, pp. 431–436.

[28] Young, W. C., and Budynas, R. G., 2002. *Roark's Formulas for Stress and Strain*, 7th ed. McGraw-Hill.

[29] Comber, D. B., Slightam, J. E., Gervasi, V. R., Neimat, J., and Barth, E. J., 2016. "Design, Additive Manufacture, and Control of a Pneumatic MR-Compatible Needle Driver". *IEEE Transactions on Robotics,* ***32***(1), pp. 138–149.

[30] Zhu, Y., and Barth, E. J., 2010. "Accurate Sub-Millimeter Servo-Pneumatic Tracking Using Model Reference Adaptive Control (MRAC)". *International Journal of Fluid Power,* ***11***(2), pp. 49–57.

[31] Richer, E., and Hurmuzlu, Y., 2000. "A High Performance Pneumatic Force Actuator System: Part 1 - Nonlinear Mathematical Model". *ASME Journal of Dynamic Systems, Measurement, and Control,* ***122***(3), pp. 416–425.